Sharp bending and power distribution of a focused radially polarized beam by using silicon nanoparticle dimers

FU DENG, HONGFENG LIU, MINGCHENG PANMAI, AND SHENG LAN[*]

Guangdong Provincial Key Laboratory of Nanophotonic Functional Materials and Devices, School of Information and Optoelectronic Science and Engineering, South China Normal University, Guangzhou 510006, China

[*]*slan@scnu.edu.cn*

Abstract: Control and manipulation of radiation direction and directivity is highly desirable in future integrated optical circuits. Here, we investigate theoretically and numerically the scattering properties of a silicon nanosphere dimer illuminated by a focused radially polarized beam. As compared with single silicon nanospheres, a scattering peak with a significantly enhanced intensity and a dramatically reduced linewidth was observed in the scattering spectrum of the silicon nanosphere dimer. Relying on the multipole expansion method, it was revealed that the radiation at the scattering peak originates mainly from the total electric dipole and the magnetic quadrupole excited in the silicon nanosphere dimer. It was found that the radiation direction of the silicon dimer is parallel to its axis, implying a sharp (90°) bending of the radially polarized beam. In addition, the radiation directivity is significantly improved as compared with single silicon nanospheres because of the interference between the total electric dipole and magnetic quadrupole modes. For a homodimer composed of two identical silicon nanospheres, the scattering light is equally distributed in the two radiation directions. In comparison, the incident light is preferentially scattered to the small Si nanosphere for a heterodimer composed of two silicon nanospheres with different diameters. As a result, a unidirectional lateral scattering can be realized by using a single silicon nanosphere displaced appropriately from the focal point. Our findings are helpful for understanding the mode hybridization in silicon nanosphere dimers illuminated by a focused radially polarized beam and useful for designing photonic devices capable of manipulating the radiation direction and directivity of structured light.

References and links

1. A. I. Kuznetsov, A. E. Miroshnichenko, Y. H. Fu, J. Zhang, and B. Luk'yanchuk, "Magnetic light," Sci. Rep. **2**, 492 (2012).
2. A. B. Evlyukhin, S. M. Novikov, U. Zywietz, R. L. Eriksen, C. Reinhardt, S. I. Bozhevolnyi, and B. N. Chichkov, "Demonstration of magnetic dipole resonances of dielectric nanospheres in the visible region," Nano Lett. **12**(7), 3749-3755 (2012).
3. A. B. Evlyukhin, C. Reinhardt, A. Seidel, B. S. Luk'yanchuk, and B. N. Chichkov, "Optical response features of Si-nanoparticle arrays," Phys. Rev. B: Condens. Matter Mater. Phys. **82**(4), 045404 (2010).
4. L. Shi, T. U. Tuzer, R. Fenollosa, and F. Meseguer, "A new dielectric metamaterial building block with a strong magnetic response in the sub-1.5-micrometer region: silicon colloid nanocavities," Adv. Mater. **24**(44), 5934-5938 (2012).
5. A. I. Kuznetsov, A. E. Miroshnichenko, M. L. Brongersma, Y. S. Kivshar, and B. Luk'yanchuk, "Optically resonant dielectric nanostructures," Science **354**(6314), 2472 (2016).
6. J. M. Geffrin, B. García-Cámara, R. Gómez-Medina, P. Albella, L. S. Froufe-Pérez, C. Eyraud, A. Litman, R. Vaillon, F. González, M. Nieto-Vesperinas, J. J. Sáenz, and F. Moreno, "Magnetic and electric coherence in forward- and back-scattered electromagnetic waves by a single dielectric subwavelength sphere," Nat. Commun. **3**(6), 1171 (2012).
7. U. Zywietz, A. B. Evlyukhin, C. Reinhardt, and B. N. Chichkov, "Laser printing of silicon nanoparticles with resonant optical electric and magnetic responses," Nat. Commun. **5**, 3402 (2014).
8. U. Zywietz, M. K. Schmidt, A. B. Evlyukhin, C. Reinhardt, J. Aizpurua, and B. N. Chichkov, "Electromagnetic Resonances of Silicon Nanoparticle Dimers in the Visible," Acs Photonics **2**(7), 913-920 (2015).

9. M. Kerker, D. S. Wang, and C. L. Giles, "Electromagnetic scattering by magnetic spheres," J. Opt. Soc. Am. **73**(6), 765-767 (1983).
10. Y. H. Fu, A. I. Kuznetsov, A. E. Miroshnichenko, Y. F. Yu, and B. Luk'yanchuk, "Directional visible light scattering by silicon nanoparticles," Nat. Commun. **4**, 1527 (2013).
11. S. Person, M. Jain, Z. Lapin, J. J. Sáenz, G. Wicks, and L. Novotny, "Demonstration of zero optical backscattering from single nanoparticles," Nano Lett. **13**(4), 1806-1809 (2013).
12. L. Wei, N. Bhattacharya, and H. P. Urbach, "Adding a spin to Kerker's condition: angular tuning of directional scattering with designed excitation," Opt. Lett. **42**(9), 1776-1779 (2017).
13. P. D. Terekhov, K. V. Baryshnikova, A. S. Shalin, A. Karabchevsky, and A. B. Evlyukhin, "Resonant forward scattering of light by high-refractive-index dielectric nanoparticles with toroidal dipole contribution," Opt. Lett. **42**(4), 835-838 (2017).
14. A. E. Krasnok, C. R. Simovski, P. A. Belov, and Y. S. Kivshar, "Superdirective dielectric nanoantennas," Nanoscale **6**(13), 7354-7361 (2014).
15. J. Q. Li, N. Verellen, D. Vercruysse, T. Bearda L. Lagae, and P. V. Dorpe, "All-dielectric antenna wavelength router with bidirectional scattering of visible light," Nano Lett. **16**(7), 4396-4403 (2016).
16. W. Liu, "Ultra-directional super-scattering of homogenous spherical particles with radial anisotropy," Opt. Express **23**(11), 14734-14743 (2015).
17. B. A. Basharin, M. Kafesaki, E. N. Economou, C. M. Soukoulis, V. A. Fedotov, Vassili Savinov, and N. I. Zheludev, "Dielectric Metamaterials with Toroidal Dipolar Response," Phys. Rev. X **5**(1), 1 (2015).
18. A. E. Miroshnichenko, A. B. Evlyukhin, Y. F. Yu, R. M. Bakker, A. Chipouline, A. I. Kuznetsov, B. Luk'yanchuk, B. N. Chichkov, and Y. S. Kivshar, "Nonradiating anapole modes in dielectric nanoparticles," Nat. Commun. **6**, 8069 (2015).
19. W. Liu, J. F. Zhang, and A. E. Miroshnichenko, "Toroidal dipole-induced transparency in core-shell nanoparticles," Laser Photon. Rev. **9**(5), 564-570 (2015).
20. L. Wei, Z. Xi, N. Bhattacharya, and H. P. Urbach, "Excitation of the radiationless anapole mode," Optica **3**(8), 799 (2016).
21. J. S. Totero Gongora, A. E. Miroshnichenko, Y. S. Kivshar, and A. Fratalocchi, "Anapole nanolasers for mode-locking and ultrafast pulse generation," Nat. Commun. **8**, 15535 (2017).
22. T. Feng, Y. Xu, W. Zhang, and A. E. Miroshnichenko, "Ideal magnetic dipole scattering," Phys. Rev. Lett. **118**(17), 173901 (2017).
23. Y. Tsuchimoto, T. A. Yano, T. Hayashi, and M. Hara, "Fano resonant all-dielectric core/shell nanoparticles with ultrahigh scattering directionality in the visible region," Opt. Express **24**(13), 14451-14462 (2016).
24. P. Albella, M. A. Poyli, M. K. Schmidt, S. A. Maier, F. Moreno, J. J. Sáenz, and J. Aizpurua, "Low-loss electric and magnetic field-enhanced spectroscopy with subwavelength silicon dimers," J. Phys. Chem. C **117**(26), 13573-13584 (2013).
25. H. Wang, P. Liu, Y. Ke, Y. K. Su, L. Zhang, N. S. Xu, S. Z. Deng, and H. J. Chen, "Janus magneto-electric nanosphere dimers exhibiting unidirectional visible light scattering and strong electromagnetic field enhancement," ACS Nano **9**(1), 436-448 (2015).
26. J. H. Yan, P. Liu, Z. Y. Lin, H. Wang, H. J. Chen, C. X. Wang, and G. W. Yang, "Directional Fano resonance in a silicon nanosphere dimer," ACS Nano **9**(3), 2968-2980 (2015).
27. D. S. Filonov, A. P. Slobozhanyuk, A. E. Krasnok, P. A. Belov, E. A. Nenasheva, B. Hopkins, A. E. Miroshnichenko, and Y. S. Kivshar, "Near-field mapping of Fano resonances in all-dielectric oligomers," Appl. Phys. Lett. **104**(2), 021104 (2014).
28. A. E. Miroshnichenko and Y. S. Kivshar, "Fano resonances in all-dielectric oligomers," Nano Lett. **12**(12), 6459-6463 (2012).
29. B. Hopkins, A. N. Poddubny, A. E. Miroshnichenko, and Y. S. Kivshar, "Revisiting the physics of Fano resonances for nanoparticle oligomers," Phys. Rev. A **88**(5), 053819 (2013).
30. M. Neugebauer, T. Bauer, P. Banzer, and G. Leuchs, "Polarization tailored light driven directional optical nanobeacon," Nano Lett. **14**(5), 2546-2551 (2014).
31. S. Roy, K. Ushakova, Q. van den Berg, S. F. Pereira, and H. P. Urbach, "Radially polarized light for detection and nanolocalization of dielectric particles on a planar substrate," Phys. Rev. Lett. **114**(10), 103903 (2015).
32. P. Wozniak, P. Banzer, and G. Leuchs, "Selective switching of individual multipole resonances in single dielectric nanoparticles," Laser Photon. Rev. **9**(2), 231-240 (2015).
33. T. Das, P. P. Iyer, R. A. DeCrescent, J. A. Schuller, "Beam engineering for selective and enhanced coupling to multipolar resonances," Phys. Rev. B: Condens. Matter Mater. Phys. **92**, 241110 (2015).
34. M. Neugebauer, P. Woźniak, A. Bag, G. Leuchs, and P. Banzer, "Polarization controlled directional scattering for nanoscopic position sensing," Nat. Commun. **7**, 11286 (2016).
35. Z. Xi, L. Wei, A. J. L. Adam, and H. P. Urbach, "Broadband active tuning of unidirectional scattering from nanoantenna using combined radially and azimuthally polarized beams," Opt. Lett. **41**(1), 33-36 (2016).
36. T. Das and J. A. Schuller, "Dark modes and field enhancements in dielectric dimers illuminated by cylindrical vector beams," Phys. Rev. B: Condens. Matter Mater. Phys. **95**(20), 201111 (2017).
37. L. Novotny and B. Hecht, *Principles of Nano-optics* (Cambridge University, 2012).
38. A commercial software developed by Lumerical Solutions Inc. (https://www.lumerical.com) is used for the numerical

simulations.

39. M. Mansuripur, "Distribution of light at and near the focus of high-numerical-aperture objectives," J. Opt. Soc. Am. A **3**, 2086-2093 (1986).

40. A. B. Evlyukhin, T. Fischer, C. Reinhardt, and B. N. Chichkov, "Optical theorem and multipole scattering of light by arbitrarily shaped nanoparticles," Phys. Rev. B: Condens. Matter Mater. Phys. **94**(20), 205434 (2016).

41. E. D. Palik, *Handbook of Optical Constants of Solids* (Academic, 1985).

42. C. J. R. Sheppard, T. X. Hoang, and X. Chen, "Multipole theory for tight focusing of polarized light, including radially polarized and other special cases," J. Opt. Soc. Am. A **29**(1), 32-43 (2012).

43. G. W. Lu, Y. W. Wang, R. Y. Y. Chou, H. M. Shen, Y. H. He, Y. Q. Cheng, and Q. H. Gong, "Directional side scattering of light by a single plasmonic trimer," Laser Photon. Rev. **9**(5), 530-537 (2015).

1. Introduction

In recent years, dielectric nanoparticles with high refractive indices have received intensive studies due to their intriguing anisotropic scattering properties originated from their intrinsic optical electric and magnetic dipole (ED and MD) resonances [1–8]. Due to the MD induced by a strong circular displacement current in the volume of such a dielectric nanoparticle, the effective magnetic polarizability can be comparable to or even stronger than the corresponding electric polarizability, resulting in the strong scattering of white light which is termed as "magnetic light". Due to the existence of multipole modes and the interference between them, dielectric nanoparticles with high refractive indices exhibit very interesting scattering properties. For instance, the coherent interaction of the ED and MD modes induced in a silicon (Si) nanosphere (NS) leads to a significantly enhanced forward scattering and considerably suppressed backward scattering or vice versus at the wavelengths where the first and second Kerker's conditions are satisfied [9–13]. In addition, the constructive interference of the ED and electric quadrupoles (EQ) modes can be employed to realize highly directional scattering into different directions [14–16]. More interestingly, the destructive interference of a Cartesian dipole and a toroidal dipole (TD) in the far field can exploited to create a nonradiative anapole mode [17–22]. In general, the scattering properties of such dielectric nanoparticles depend strongly on their shapes [13–16, 23]. In addition, the assembling of a few dielectric nanoparticles into dimers or oligomers can also be employed to realize photonic devices with desirable radiation properties [24–29]. Alternatively, structured light can be used to modify the optical responses of dielectric nanoparticles [30–36].

A focused radially polarized (RP) beam, which possesses an electric field in the propagation direction [37], excites only the electric modes of a nanoparticle placed at the focal point and suppresses all the magnetic modes [20, 32–34]. As compared with a linearly polarized beam, only the coupling efficiencies of the incident light to the electric and magnetic modes of the nanoparticle are modified and the underlying multipolar spectral line shapes remain unchanged [33]. The nonradiative anapole mode, which is created by the destructive interference of the ED and TD modes in the far field [17–19], can be observed directly for a Si NS placed at the focal point of a focused RP beam because the magnetic modes are suppressed [20]. Since only the longitudinal ED is excited in the Si NS placed at the focal point, the radiation of the Si NS exhibits azimuthal omnidirectionality in the transverse plane with no scattering in the forward direction. When the Si NS is moved away from the focal point, both the electric and magnetic modes can be excited in the Si NS, leading to a unidirectional lateral scattering which originates from the interference of the longitudinal ED and the transverse ED and MD modes [34].

Owing to the different nature of mode hybridization, the scattering spectrum of a dielectric nanoparticle dimer under a cylindrical vector beam illumination is qualitatively different from that under a plane wave illumination. Very recently, the dark modes and field enhancements in a dielectric nanoparticle dimer under a cylindrical vector beam illumination has been investigated [36].

In this work, we unveil the mode hybridization in a Si NS dimer under the illumination of a RP beam by using the Cartesian multipole decomposition method. It is found that the constructive

interference between the ED and TD modes leads to the formation of a TED mode which generates a scattering peak with significantly enhanced scattering intensity and dramatically reduced linewidth. In addition, it is revealed that the interference of the TED mode with a MQ mode originating from the discontinuous magnetic flux loop results in the bidirectional scattering along the axis of the dimer. The existence of the an electric field component Ez in the propagation direction plays a crucial role in realizing the sharp bending, which cannot be achieved for linearly polarized beam. It is shown that a MD mode is induced in a heterodimer composed of two Si NSs with different diameters owing to the breaking of the structural symmetry, and the scattering occurs preferentially to the direction of the small Si NS.
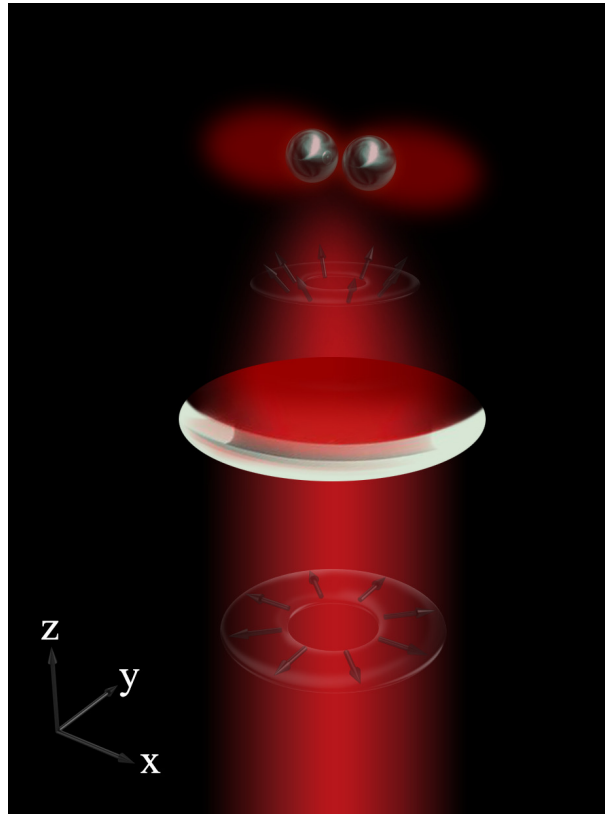

Fig. 1. Schematic showing the excitation of a Si NS dimer with a focused RP beam and the radiation of the Si NS dimer along its axis. The Si NS dimer is composed of two Si NSs with the same radius of $r_1 = r_2 = 100\ nm$ and separated by a distance of $g = 20\ nm$ in the x direction. The RP beam is propagating along the $+z$ direction.

In Fig. 1, we show schematically the excitation of a Si NS dimer with a RP beam and the resulting radiation of the Si NS dimer. The two Si NSs in the dimer have the same radius of $r_1 = r_2 = 100\ nm$ and they are separated by a distance of $g = 20\ nm$ in the x direction. The RP beam is propagating along the $+z$ direction and the axis of the dimer is along the x direction. The numerical aperture (NA) of the objective lens used to focus the RP beam is chosen to be 0.86, corresponding to a focusing angle of $\alpha = \pm 60°$.

2. Numerical methods

The scattering spectra of the Si NS dimers discussed in this work were simulated by using the finite-difference time-domain (FDTD) technique [38]. In the numerical implementation, the focal field of the radially polarized beam with a diameter of 300 *nm* at the focal plane is calculated by the *k*-space beam profile definition [39] and then imported to FDTD simulation. In order to obtain the scattering spectrum of a Si NS dimer, we first computed the background field of the RP beam in the absence of the Si NS dimers by using the FDTD simulation via the cross section analysis group. Then, the total field in the presence of the Si NS dimers was calculated. Finally, the scattering field was derived from the difference between the total field and the background field. The decomposition of the scattering spectra into the contributions of various electric and magnetic modes was performed by using the multipole expansion method [40]. The dielectric function of Si was obtained from Palik [41] and the surrounding medium is set as air. A mesh size of 2 *nm* was used for the illuminated region. Perfectly matched layers were used at the boundary to terminate the finite simulation region. We have also performed numerical simulations for Si NS dimers placed on a glass substrate. It was found that the influence of the glass substrate on the scattering properties of Si NS dimers is negligible because of the relatively small refractive of the glass substrate ($n \sim 1.45$) with respect to the Si NSs ($n \sim 3.4$).

3. Results and discussion

In Fig. 2(a), we present the scattering spectrum of the Si NS dimer shown in Fig. 1 ($r_1 = r_2 = 100$ *nm*) calculated by using the FDTD simulation. For comparison, the scattering spectrum of a single Si NS placed at the focal point is also shown. It can be seen that all the magnetic modes are suppressed and only the electric modes are excited for the single Si NS. In addition, the anapole mode which is formed by the destructive interference of the ED and TD modes in the far field is also excited, resulting in a scattering dip at ~560 *nm* with the weak contribution of the EQ mode [20]. These phenomenons, which have been reported in previous literatures [20, 32–34], can be explained explicitly by using the multipole theory for tightly focused RP beam [42] whose electric field is described as follows:

$$\mathbf{E_f}\left(\mathbf{r}\right) = \sum_{l=1}^{\infty} \left[p_{El}^0 N_l^0\left(\mathbf{r}\right) + p_{Ml}^0 M_l^0\left(\mathbf{r}\right) \right]. \tag{1}$$

Here, p_{El}^0 and p_{Ml}^0 are the strengths of the electric and magnetic components, which have been analytically calculated by using Eq. (10) in the previous work [42]. For a RP beam, we can get $p_{Ml}^0 = 0$, implying that all the magnetic multipole components are suppressed. In Fig. 2(a), it can be seen that the scattering spectrum of the Si NS dimer is quite different from that of the single Si NS due to the different nature of mode hybridization. Apart from the weak scattering peak appearing at ~600 *nm*, one can see a strong scattering peak located at ~790 *nm*. The narrower linewidth of ~40 *nm* observed for the scattering peak implies an efficient scattering or radiation from the Si NS dimer. In this work, we will identify the physical origin of this scattering peak and investigate the radiation behavior of the Si NS dimer at this resonance.

In order to understand the physical origin of the resonant peak at ~790 *nm*, we employed the multipole expansion method [18, 40] to decompose the total scattering spectrum of the Si NS dimer into the contributions of various electric and magnetic modes, as shown in Fig. 2(b). Basically, the multipolar decomposition starts from the polarization $\mathbf{P} = \varepsilon_0\left(\varepsilon_p - \varepsilon_d\right)\mathbf{E}$ induced by the incident light, where $\mathbf{E}$ is the total electric field inside the particle, ε_0, ε_p, ε_d are the vacuum dielectric constant, relative dielectric permittivity of the particle, and relative dielectric permittivity of the surrounding medium, respectively.

The multipoles are defined in a Cartesian coordinate with the origin located at the center of mass of the dimer. The multipole moments can be obtained by the integration of the induced

polarization currents over the volume of the dimer. The ED moment is expressed as:

$$\mathbf{p} = \int_V \varepsilon_0 \left(\varepsilon_p - \varepsilon_d \right) \mathbf{E}\left(\mathbf{r}'\right) d\mathbf{r}', \tag{2}$$

where V is the scatterer volume and $\mathbf{r}'$ is the radius vector of a volume element inside the particle.

The TD moment is described as:

$$\mathbf{T} = \frac{i\omega}{10} \int_V \left\{ 2\mathbf{r}'^2 \mathbf{P}\left(\mathbf{r}'\right) - \left[\mathbf{r}' \cdot \mathbf{P}\left(\mathbf{r}'\right)\right] \mathbf{r}' \right\} d\mathbf{r}'. \tag{3}$$

The MD moment is given by:

$$\mathbf{m} = -\frac{i\omega}{2} \int_V \left[\mathbf{r}' \times \mathbf{P}\left(\mathbf{r}'\right)\right] d\mathbf{r}'. \tag{4}$$

The irreducible EQ and magnetic quadrupole (MQ) tensors ($\widehat{U}$ is the 3×3 unittensor) are derived by:

$$\widehat{Q} = 3 \int_V \left\{ \mathbf{r}'\mathbf{P}\left(\mathbf{r}'\right) + \mathbf{P}\left(\mathbf{r}'\right)\mathbf{r}' - \frac{2}{3}\left[\mathbf{r}' \cdot \mathbf{P}\left(\mathbf{r}'\right)\right]\widehat{U} \right\} d\mathbf{r}'. \tag{5}$$

$$\widehat{M} = \frac{\omega}{3i} \int_V \left\{ \left[\mathbf{r}' \times \mathbf{P}\left(\mathbf{r}'\right)\right]\mathbf{r}' + \mathbf{r}'\left[\mathbf{r}' \times \mathbf{P}\left(\mathbf{r}'\right)\right] \right\} d\mathbf{r}'. \tag{6}$$
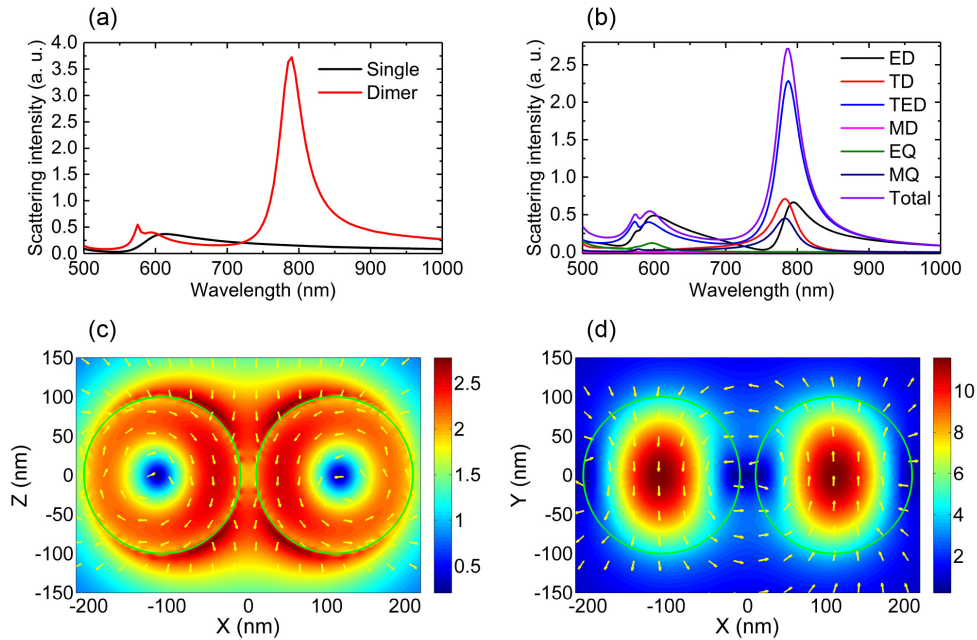

Fig. 2. (a) Total scattering spectrum (red curve) calculated for the Si NS dimer illuminated by a RP beam. The scattering spectrum of a single Si NS placed at the focal point (black curve) is also provided for comparison. (b) Multipolar decomposition of the scattering spectrum of the Si NS dimer into the contributions of various electric and magnetic modes. The electric and magnetic field distributions calculated at the scattering peak (790 *nm*) of the Si NS dimer are presented in (c) and (d), respectively.

The interference of the ED and TD moments can be treated as the total electric dipole moment (TED) $\mathbf{p} + \frac{ik_0\varepsilon_d}{c}\mathbf{T}$ with the wave number k_0 and light velocity c in vacuum. When all the multipole

moments mentioned above are taken into account, the total scattering cross section σ_{sca} can be written as [40]:

$$\sigma_{\text{sca}} = \frac{k_0^4}{6\pi\varepsilon_0^2|\text{E}_{inc}|^2}\left|\mathbf{p} + \frac{ik_0\varepsilon_d}{c}\mathbf{T}\right|^2 + \frac{k_0^4\varepsilon_d\mu_0}{6\pi\varepsilon_0|\text{E}_{inc}|^2}|\mathbf{m}|^2$$
$$+\frac{k_0^6\varepsilon_d}{720\pi\varepsilon_0^2|\text{E}_{inc}|^2}\sum_{\alpha\beta}|Q_{\alpha\beta}|^2 + \frac{k_0^6\varepsilon_d^2\mu_0}{80\pi\varepsilon_0|\text{E}_{inc}|^2}\sum_{\alpha\beta}|M_{\alpha\beta}|^2, \tag{7}$$

where μ_0 is the vacuum permeability, and the indexes $\alpha = x, y, z$ and $\beta = x, y, z$.

From the multipolar decomposition of the scattering cross section of the Si NS dimer shown in Fig. 2(b), it is noticed that the interference of the ED and TD modes is constructive, which generates a super-dipole mode (i.e., TED) [13] corresponding to the resonant peak at ~790 *nm*. In addition, a MQ resonance located at ~780 *nm*, which is absent for a single Si NS illuminated with a RP beam [20, 32–34], also contributes to the scattering peak at ~790 *nm*. Physically, the MQ mode is induced by the discontinuous magnetic flux loop which leads to the formation of two anti-parallel MD moments while the TD mode is characterized by the circulating magnetic flux along the closed loop [18]. Therefore, the strong resonant peak observed in the scattering spectrum is actually the superposition of the TED and MQ resonances [see Fig. 2(b)]. In Figs. 2(c) and 2(d), we show the electric and magnetic field distributions on the XZ and XY planes calculated at the resonant peak of ~790 *nm*. In Fig. 2(c), we observe circular displacement currents of clockwise and anti-clockwise in the left and right NSs, respectively. As a result, the electric field in the gap region of the dimer is along the *z* axis and a circular magnetic field distribution is observed on the XY plane, as shown in Figs. 2(c) and 2(d). It is the circular magnetic field that generates a TD mode oriented in the *z* direction. Thus, the existence of the TD mode in the scattering spectrum is confirmed by the magnetic field distribution of the Si NS dimer.

Now, it becomes clear that the enhanced scattering observed in a homodimer illuminated by using a RP beam originates from the interference of the TED and MQ modes. As compared with the homodimer, the mode hybridization in a heterodimer is more complicated because of the asymmetrical structure of the heterodimer with respect to the RP beam. In Fig. 3(a), we show the scattering spectra calculated for a few heterodimers with the same gap width of $g = 20$ *nm*. In each case, the radius of the right Si NS is kept unchanged ($r_1 = 100$ *nm*). It is found that the resonant peak is blueshifted or redshifted when the radius of the left Si NS is reduced or increased. In all cases, a reduction in the scattering intensity as well as a broadening of the linewidth is observed, as shown in Fig. 3(a).

In order to understand how the asymmetric structure of a heterodimer influences the scattering behavior, the scattering spectra of two heterodimers with $r_2 = 90$ and 110 *nm* are decomposed, as shown in Figs. 3(b) and 3(c). Different from the scattering spectrum of a homodimer in which the MD mode absent, the scattering spectrum of a heterodimer involves a significant contribution of the MD mode. Since the radii of the two Si NSs are different in the heterodimer, the MD$_y$ modes induced in the two Si NSs are not canceled out, leaving a non-zero MD mode which contributes significantly to the resonant peak in the scattering spectrum. Therefore, the radiation of a heterodimer is determined by the interference of the TED, MQ and MD modes.

In Fig. 4(a), we show the three-dimensional (3D) radiation pattern simulated for the homodimer with $r_1 = r_2 = 100$ *nm* at the resonant peak of ~790 *nm* by using the FDTD simulation. It can be seen that a bidirectional scattering along the *x* axis of the dimer is achieved. In this case, the bending efficiency of the homodimer, which is defined as the power of the scattering light in the *x* direction divided by that of the total scattering light in all directions, is calculated to be 43.5%. For heterodimers, it is expected that the power distributions in the two radiation directions are
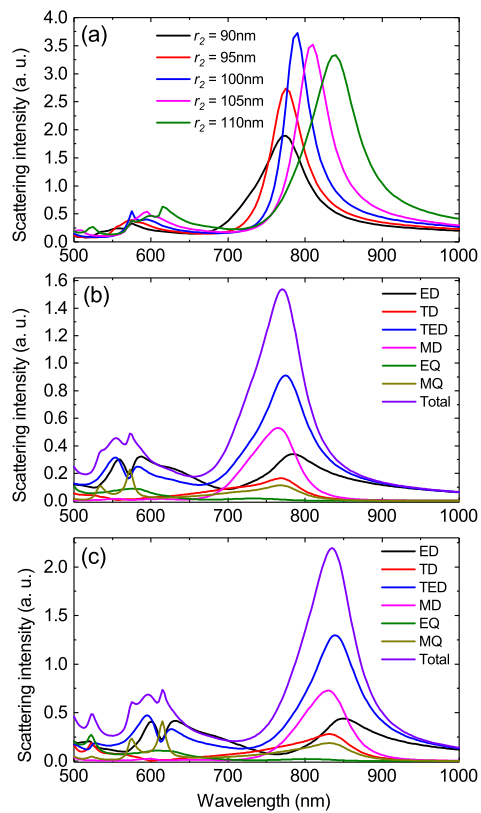
Fig. 3. (a) Scattering spectra calculated for heterodimers with $r_1 = 100\ nm$ and $r_2 = 90, 95,$ 105, and 110 nm. The scattering spectrum of the homodimer with $r_1 = r_2 = 100\ nm$ is also provided for comparison. The decompositions of the scattering spectra for the hetrodimers with $r_2 = 90$ and 110 nm are shown in (b) and (c).

different because of the breaking of the structural symmetry, as shown in Figs. 4(b) where the two-dimensional (2D) radiation patterns on the XY plane for the heterodimers with $r_2 = 90$ and 110 *nm* excited at the resonant peaks are presented. In both cases, it can be seen that the incident light is preferentially scattered to the small Si NS.
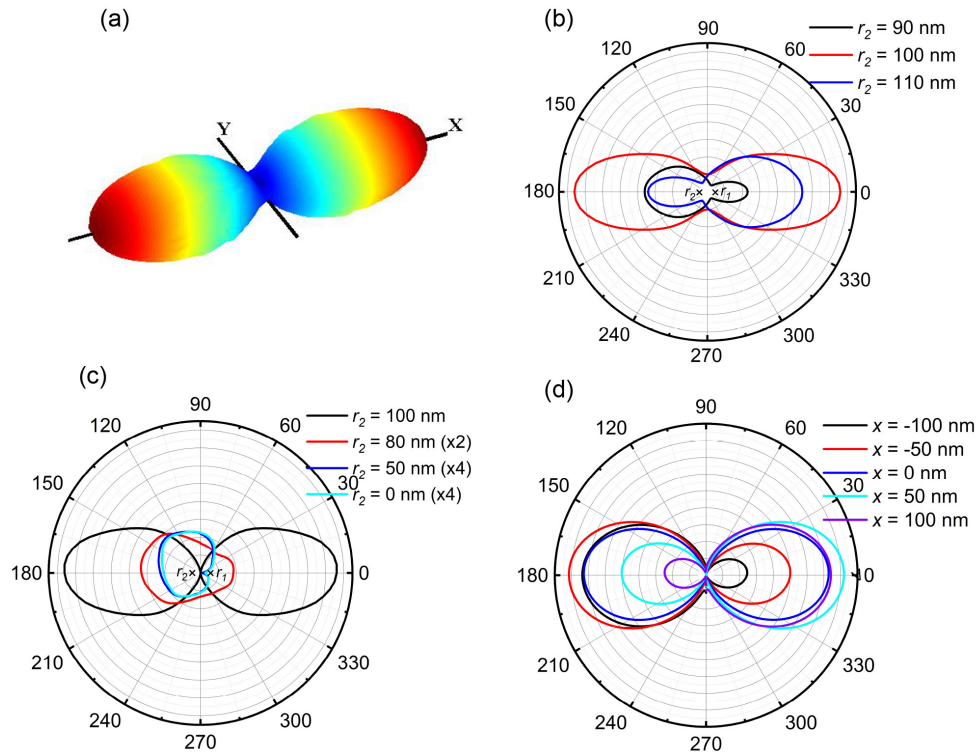

Fig. 4. (a) 3D radiation pattern of a homodimer with $r_1 = r_2 = 100$ *nm* illuminated by using a RP beam. (b) 2D radiation patterns on the XY plane calculated for heterodimers with $r_2 = 90$ and 110 *nm*. The 2D radiation pattern of a homodimer with $r_1 = r_2 = 100$ *nm* is also provided for comparison. (c) 2D radiation patterns on the XZ plane calculated for heterodimers with decreasing the radius of the left sphere. The 2D radiation pattern of a homodimer with $r_1 = r_2 = 100$ *nm* and a single Si NS displaced 110 *nm* away from the focal point of the RP beam are also provided for comparison. The symbols × in (b) and (c) indicate the positions of the Si NSs. (d) 2D radiation patterns on the XZ plane calculated for a homodimer ($r_1 = r_2 = 100$ *nm*) whose center is shifted away from that of the RP beam in the *x* direction by different values.

In Fig. 4(c), we show the 2D radiation patterns on the XZ plane calculated for heterodimers with $r_2 = 80, 50$ and 0 *nm*. It is remarkable that power distributions in the two radiation directions become more asymmetric with decreasing the radius of the small Si NS. When the radius of the small Si NS is reduced to zero (i.e., a single Si NS displaced from the focal point of the RP beam), a unidirectional lateral scattering can be achieved. It is noticed, however, the radiation directivity of the single Si NS is greatly reduced as compared with that of the Si NS dimer. In this case, the radiation pattern can be modified by controlling the relative position of the Si NS to the focal point, as demonstrated in previous literature [34]. For a heterodimer, it should be emphasized that the interacting wavelength of the multipoles no longer coincides with the resonant wavelength of the scattering spectrum. In Fig. 4(d), we show the 2D radiation patterns on the XZ plane calculated for a homodimer ($r_1 = r_2 = 100$ *nm*) whose center is shifted away from that of the RP

beam in the x direction by different values. Similar to the situation of heterodimers, it can be seen that unidirectional lateral scattering in the x direction can also be achieved in the homodimer when the shift of its center from that of the RP beam exceeds 100 nm.
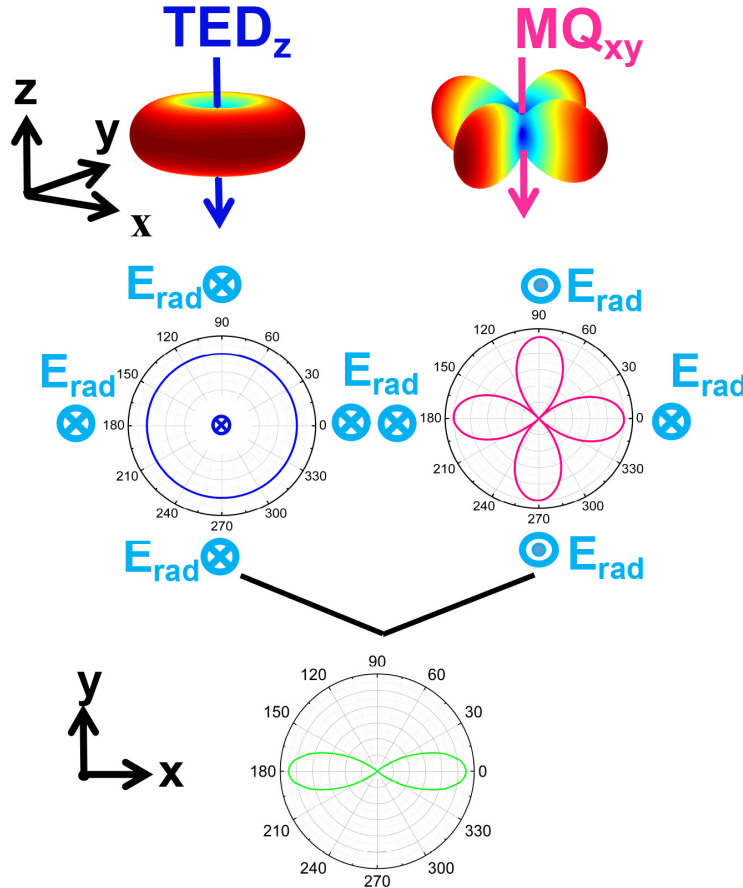

Fig. 5. 3D and 2D radiations patterns calculated for the TED_z and MQ_{xy} modes interacting coherently (see the first and second rows). The radiation pattern resulting from the interference of the TED_z and MQ_{xy} modes is also schematically shown (see the third row).

The achievement of the radiation patterns shown in Fig. 4 can be understood qualitatively from the interference of the radiation patterns of the electric and magnetic modes interacting coherently, as schematically shown in Figs. 5 and 6. For a homodimer, the radiation pattern is determined by the interference of the TMD_z and MQ_{xy} modes. Consequently, the interference leads to the bidirectional radiation in the x direction, as shown in Fig. 4. In addition, a good directivity is observed because the radiation originates from the interaction of a dipole and a quadrupole modes [15]. Since the amplitude of the MQ mode is smaller than that of the TED mode, the destructive interference in the y direction is not complete, leading to the non-zero radiation in the y direction [see Fig. 4]. In a heterodimer, the radiation is determined by the interference between the TED_z and MD_y modes, which is quite similar to the radiation of a single Si NS, as shown in Fig. 6. Different from a single Si NS illuminated by using a plane wave, however, the radiation of the heterodimer illuminated by using a RP beam appears in the x direction instead of the z direction. Moreover, the transverse TED_x mode should be taken

into account when the radius of the small Si NS becomes smaller than 50 *nm*. In this case, the interference of TED_z, MD_y and TED_x modes leads to a unidirectional lateral scattering with deteriorate radiation directivity [see Fig. 4(c)].
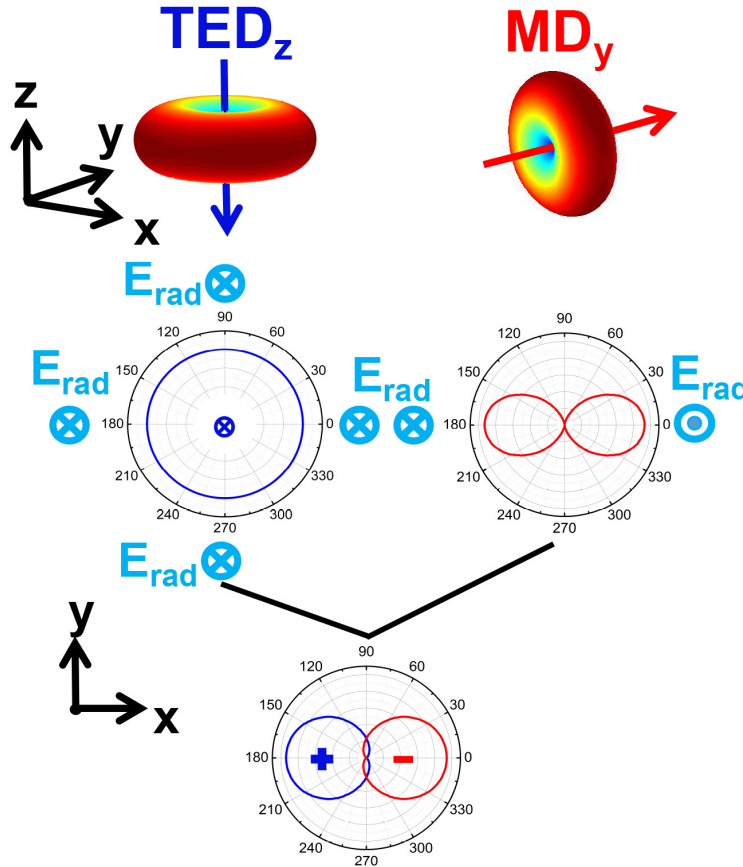

Fig. 6. 3D and 2D radiations patterns calculated for the TED_z and MD_{xy} modes interacting coherently (see the first and second rows). The radiation pattern resulting from the interference of the TED_z and MD_{xy} modes is also schematically shown (see the third row).

4. Conclusion

In summary, we have investigated the radiation behavior of a Si NS dimer illuminated by using a focused RP beam. A strong resonant peak with enhanced scattering intensity and reduced linewidth is observed in the scattering spectrum of the Si NS dimer. The physical origin of the resonant peak is identified by decomposing the scattering spectrum into the contributions of various electric and magnetic modes. It is revealed that the scattering of a homodimer is governed by the interference of the TED and MQ modes while that of a heterodimer is determined by the interference of the TED, MQ, and MD modes. Bidirectional radiation along the *x* axis of the dimer is observed, implying a sharp bending (90°) of the incident RP beam. Power distributions in the two radiation directions can be achieved by using a heterodimer and a unidirectional lateral scattering can be realized by using a Si NS displaced appropriately with respect to the focal point. Our finds are quiet helpful for understanding the mode hybridization in a Si NS dimer illuminated by using a RP beam and useful for designing photonic devices capable of manipulating light

radiation. In practice, the photonic device proposed in this work can be built by using the laser printing method [7, 8] in combination with the nanomanipulation method [43]. Si NSs with accurate size and position control can be fabricated on a glass substrate by using the laser printing method [7, 8]. In addition, the creation of Si dimers with controllable gap widths can be realized by using the tip of an atomic force microscope [43].

Funding